Retractable Locking System Driven by Shape Memory Alloy Actuator for Lightweight Soft Robotic Application

Young Jin Gong, Seong Taek Hwang, Sang Yul Yang, Kihyeon Kim, Jae Hyeong Park, Hosang Jung, Dongsu Shin, and Hyouk Ryeol Choi, *Fellow, IEEE*

***Abstract*—Shape memory alloy actuators (SMA) are widely used in robots owing to their flexibility and light weight. However, there is a drawback in that SMAs need to be used as a bundle owing to their lower force density than the motor. In addition, SMAs require continuous current to maintain a contracted state, which results in the overheating of the actuator, causing breakdown and excessive energy consumption. This study presents a new locking system that can mechanically hold the contracted state of an actuator without consuming energy to overcome the disadvantages of a spring-type SMA. The locking mechanism was designed with a ratchet structure and pawl to prevent the actuator from stretching in the opposite direction when locked. In addition, to switch the locking and unlocking states with a single one-way actuation, a bistable retractable mechanism was applied to the system. Repeatability experiments and an analysis of the locking system resolution were conducted to validate the performance of the proposed mechanism. Furthermore, an underactuated finger applied to the proposed locking system was fabricated, and its feasibility is experimentally presented.**

***Index Terms*—Bistable mechanism, locking mechanism and SMA spring actuator, soft robot applications, soft sensors and actuators.**

I. Introduction

THE skeletal muscles contract to move various joints in a human body. Each joint has muscles attached to it that move the joint; thus, the joints move through contraction and relaxation. Each muscle moves silently, is very sophisticated, and responds quickly. Recently, various artificial muscles, which include pneumatics, polymer fibers, and shape memory alloys, have been developed to mimic the benefits of skeletal muscles [1], [2], [3], [4], [5], [6], [7], [8]. Shape memory alloys actuator (SMA) has a high energy density and can be used in various shapes. Therefore, SMA are actively used in extensive applications and have attracted attention as next-generation actuators to replace motors [9], [10]. These SMAs can be used depending on the required force and size, while controlling the length and number of spring coils to suit the required specifications and size of the model [11], [12]. However, after the completion of operation of the SMA and cooling down, the force gets released and the actuator freely deforms, obstructing it to maintain its contraction. This flexibility is also an advantage of the SMA; however, this hampers the robotic joint from holding the object or maintaining the grip. Many locking mechanisms have been studied to solve the power management or actuator breakage problems caused by continuous energy consumption to maintain the displacement of the soft actuator, and they are believed to have potential in robot applications [13].

Saharan et al. presented a mechanical locking mechanism using an extension spring to compensate for the insufficient force of an SMA [14]. However, this mechanism consumes high power, and because of its structural properties, the spring returns to the locking position, hampering its quick response. Park et al. proposed a locking mechanism for fabric-type soft actuators with increased energy efficiency [15]. However, it is difficult to develop this mechanism for fabric actuators because of the discontinuity of its locking effect; therefore, it is difficult to maintain locked state while the actuator contracts. Hu et al. suggested a locking mechanism of the ratchet structure applied to soft robotic fingers driven by a spring-type SMA and presented an FEA analysis and modeling based on gears [16]. However, owing to the shape embedded in the finger, it cannot be scaled to other applications.

In this paper, a mechanical design of a compact locking mechanism combining a ratchet and retractable switch structure is proposed to supplement the force of the SMA and the model of the locking system when operating the actuator. In addition, the SMA was optimized to operate the locking system, and repeatability tests were conducted. Finally, to validate the feasibility of the proposed retractable locking system (RLS) as a soft robotic application, a tendon-driven underactuated finger was fabricated and lifting experiments were performed.

The remainder of this paper is organized as follows. Section II presents the design of the locking mechanism and modeling, and the operation principles of the retractable locking switch.

Manuscript received 30 August 2022; accepted 26 September 2022. Date of publication 10 October 2022; date of current version 20 October 2022. This letter was recommended for publication by Associate Editor P. Chirarattananon and Editor Y.-L. Park upon evaluation of the reviewers' comments. This work was supported by the National Research Foundation of Korea (NRF) funded by the Korea Government (MSIT) under Grants 2020R1A4A1018227 and 2021R1A2C3012387. *(Corresponding author: Hyouk Ryeol Choi).*

The authors are with the School of Mechanical Engineering, Sungkyunkwan University, Suwon 2066, South Korea (e-mail: youngjin510@skku.edu; tjdxor05@skku.edu; didtkddbf@skku.edu; kimkh0471@g.skku.edu; csp00275@skku.edu; jhsx1004@skku.edu; anaud94@skku.edu; choihyoukryeol@gmail.com).

This letter has supplementary downloadable material available at https://doi.org/10.1109/LRA.2022.3213489, provided by the authors.

Digital Object Identifier 10.1109/LRA.2022.3213489

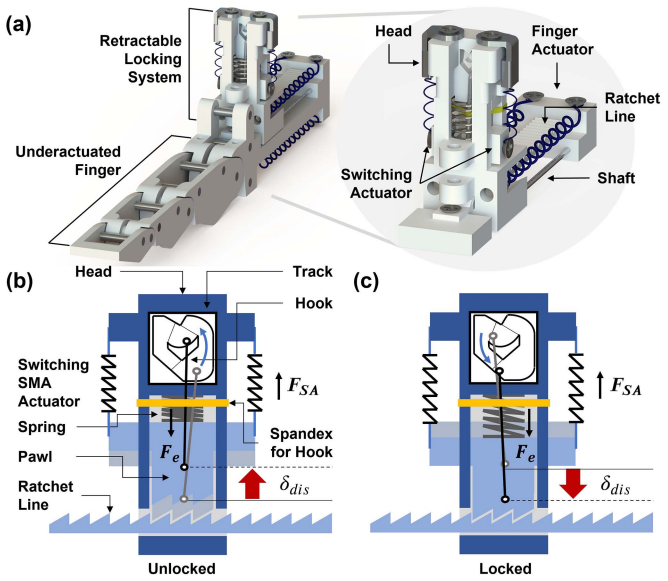

Fig. 1. (a) Concept of retractable locking system (RLS) and its soft robotic application (Tendon driven underactuated finger module), (b) Switch diagram and force analysis when the pawl moves vertically. Pawl is raised by force $\boldsymbol{F_{SA}}$ generated by switching SMA when RLS is unlocked, (c) Falling pawl owing to spring elasticity $\boldsymbol{F_e}$ when RLS is locked.

Section III presents the proposed underactuated mechanism, locking system, and lifting experiments. Finally, Section IV concludes the study.

II. Mechanism Design of Retractable Locking System

A. Ratchet and Retractable Switch Mechanism

In this study, a locking system with a ratchet mechanism is presented to complement the force of the spring-type SMA that exerts instantaneous linear displacement and force when heated. The ratchet used in this study allows only one-way movement when a gear is engaged, and its locking force occurs between the pawl and ratchet lines. The proposed locking system with a ratchet line was applied to supplement the force generated by the SMA operating in the soft robotic system that maintains the contraction position. However, to apply this mechanism to robotic joints requiring bidirectional movement, a switch is required that locks and unlocks ratchet only when intended by the users. Therefore, a bistable retractable structure driven by a dedicated SMA has been applied to this locking system to allow it to switch between two states; thus, each time the actuator contracts, the locking and unlocking states are switched, allowing the actuator to move in both directions, as shown in Fig. 1(b) and 1(c).

Various studies have been conducted to achieve displacements with less energy and implement bistability [17]. Although this study does not have strict characteristics, such as topology or fast snap deformation of bistable structures, RLS similarly achieves displacement of the soft actuator with low energy consumption without continuous heating of the actuator and then holds it in that state. Groothuis et al. were inspired by a ball-point pen and presented a study that achieved rotational motion through the cam and follower structure and bistability within the sequence [18].

TABLE I
Values of Parameters of the RLS

Symbol	Parameter	Value (unit)
R_1	Radius of rotation of the hook	13 (mm)
δ_{dis}	Maximum displacement in the y-axis direction of the hook on track	8 (mm)
δ_{hook}	Height of hook-arresting part in y-direction	4.5 (mm)
w	Width of slope of track	1.2 (mm)
h_1	The lowest area of the track	2.5 (mm)
h_2	The second highest area of the track	3.25 (mm)
h_3	The highest area of the track	4 (mm)

The switch mechanism of the designed RLS shown in Fig. 2(a) comprised a head, pawl, and hook attached to the pawl implementing a 2 degree of freedom (DoF) cylindrical joint, track guiding the hook, ratchet line, and two spring-type SMAs for switching the pawl's position. The head, which can move along the ratchet line, was connected to a pawl, which generated a holding force while engaging with the ratchet line, to achieve vertical movements. These two parts were connected by a dedicated switching SMA (SA) and could move upward, with a spring between the two parts designed to push the pawl downward. In addition, to implement the retractable mechanism through the cam and cam follower, a hook was fixed as a cylindrical joint to the pawl, and the other end moved along the track that was dug into the head (Fig. 2(b)), which held the pawl in two stable states. Furthermore, the prestrained spandex was wound between the hook and head to ensure constant contact between the hook and track. The track had three thresholds to stop the hook from reversing after rotating counterclockwise (CCW). The track parameter values are listed in Table I.

In Fig. 2(c), the CCW movement of the hook along the track is shown. When the hook, acting as the cam follower, is in a stable position (1), the pawl is lowered, which creates the locking state of the RLS. When heat is applied to contract the SA and generate a force $\boldsymbol{F}_{SA}$, it exceeds the spring's elastic force $\boldsymbol{F}_e$ and the pawl moves upward. The hook attached to the pawl then moves up to position (2) (Figs. 1(b) and 2(e)). When the heating of the SA is stopped, $\boldsymbol{F}_{SA}$ reduces compared to $\boldsymbol{F}_e$ and the hook falls vertically to a stable position (3) (Fig. 2(f)). The lowered hook is caught in the center and allows the pawl to be fixed in an elevated state, which creates an unlocked state of the RLS. Once again, when the SA is operated, the hook moves up to position (4) (Figs. 1(c) and 2(g)). Finally, as the SAs stop, the pawl is brought down to position (1) again by the $\boldsymbol{F}_e$ (Fig. 2(h)), and the RLS is locked. In addition, after the switching process, no additional heating is required, except for the heat applied to the actuator while operating the mechanism. Therefore, the following equations were obtained:

$$F_y = \begin{cases} F_{SA} - \mu_h N_h - F_e, & \text{if SA is on} \\ \mu_h N_h - F_e, & \text{if SA is off} \end{cases} \quad (1)$$

$$N_h = T_h = k_h \delta_z + T_0 \quad (2)$$

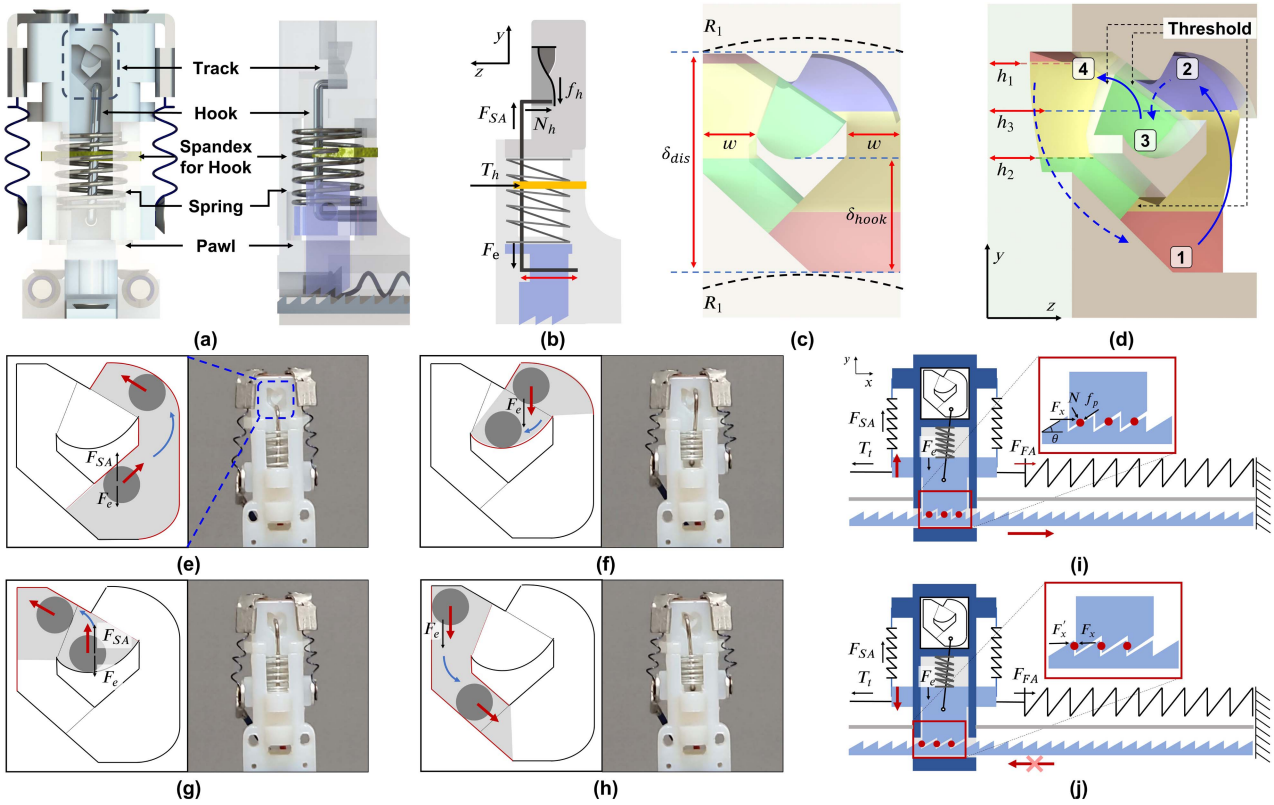

Fig. 2. (a) Detailed structure and labels of each part of switch head (Right: Front view, Left: Side view), (b) Force analysis of the hook from the side view ($\boldsymbol{f_h}$: Friction force between hook and track surface, $\boldsymbol{T_h}$: Elastic tension force of spandex for hook, and $\boldsymbol{N_h}$: Normal force applied by hook generated by spandex to track surfaces), (c),(d) Geometrical shape and three-dimensional structure of the track (Each region is represented in the z-axis direction. Red: Lowest area of the track, Green: The second highest area, Blue: The highest area, and Yellow: CCW rising slope), (e)-(h) Hook movement traveling along the track (The gray circle is the position of the hook, the colored area is the moving area of the hook, the red arrow indicates the direction of hook, and the movement trajectory is shown in blue.), (i),(j) Developed retractable locking system comprising switches, actuator for pulling switch, and ratchet lines ($\boldsymbol{f_p}$: Friction force between pawl and ratchet line, $\boldsymbol{F_x}$: Net force of $\boldsymbol{F_{FA}}$ and $\boldsymbol{T_t}$ on RLS, and $\boldsymbol{F_x'}$: Reaction force of $\boldsymbol{F_x}$).

where $\boldsymbol{F_y}$, μ_h, k_h, $\boldsymbol{\delta_z}$, and T_0 denote the net force on the hook on the y-axis, friction coefficient between the hook and track surface, spring constant of the wounded spandex, displacement of the spandex increased by the hook moving along the slope of the track surface, and tension of the prestrained spandex, respectively. Furthermore, even if the posture of the RLS changes in space and the weight of the hook acts in a different direction than the existing direction, T_h is larger than w_h because the mass of hook is 0.2 g, the spandex's spring constant is 0.0764 N·mm, which is prestrained by more than 2 mm. Moreover, $\boldsymbol{\delta_z}$ increases compared to when the hook is located in position (1) owing to the z-direction height difference by h_1, h_2 and h_3 of the track, thus the hook remains in contact with the track. Therefore, when the height difference between h_1, h_2 and h_3 increases, δ_z becomes higher, which results in greater frictional force by N_h, which makes contact of the hook with track more stable, while may interfere with the operation of the RLS. In addition, operational experiments of the RLS in different gravitational directions were conducted, which can be found in the multimedia data (Supplementary video). Therefore, the following equations were obtained:

$$T_h = k_h \delta_z + T_0 > w_h = m_h g \tag{3}$$

This means that the hook is always in contact with the track, regardless of the posture of the RLS, because the hook is only capable of z-direction rotation and translational movement in the local x-y plane. In addition, at the two stable positions (1) and (3) on the track, the hook in contact with the track is always attached to the side wall of the track when the SA is not operated by the elastic force $\boldsymbol{F_e}$ of the spring with a spring constant of 0.6 N/mm.

The proposed switch mechanism, RLS operation, has two states: locked and unlocked; however, in the latter state, it is divided into two cases depending on the direction of the force applied to the RLS, resulting in a total of three cases: when the RLS is unlocked (Case 1), and it is free to move according to the direction of the net force $\boldsymbol{F}_x$ of the force $\boldsymbol{F}_{FA}$ exerted by the finger actuator (FA) and tension T_t. When the RLS is activated and locked, the FA can be divided into relaxed and contracted cases (Case 2, 3). When the FA contracts further while being locked ($\boldsymbol{F}_{FA} > \boldsymbol{T}_t$), the actuator contracts step by step, interfering with the friction between the ratchet line and pawl (Fig. 2(i)). However, when the FA is relaxed in the direction it is intended to release ($\boldsymbol{F}_{FA} < \boldsymbol{T}_t$), the actuator is no longer relaxed by the reaction force $\boldsymbol{F}_x'$ caused by the ratchet structure (Fig. 2(j)). Unlike in the fully unlocked state, the spring force pushing down the pawl causes the actuator to contract while the

RLS remains locked. In addition, this condition can compensate for the shortcomings of SMA, which vary in the force that can be produced depending on the strain, by maintaining the locked state while contracting. Therefore, the following equations were obtained:

$$F_x = \begin{cases} F_{FA} - T_t, & (\text{Case } 1) \\ 0, & (\text{Case } 2) \\ F_{FA} - T_t - \mu_p N_p \cos\theta, & (\text{Case } 3) \end{cases} \tag{4}$$

$$N_p = F_e \cos\theta \tag{5}$$

where N_p, μ_p, $\boldsymbol{F_x}$, and θ denote the normal force applied by the pawl on the surface of the ratchet line, friction coefficient between the pawl and ratchet lines, net force on the switch head of $\boldsymbol{F_{FA}}$ and $\boldsymbol{T_t}$, and angle of inclination of a gear on a ratchet line, respectively.

B. Actuator for Retractable Switch Mechanism

The switch mechanism of the RLS operates with a fixed displacement along a moving line. Because the switching of RLS works through the SA made up of SMA springs (artificial muscle, Flexinol Co, spring diameter: 2.54 mm and wire diameter: 0.381 mm), the system can be configured with a light weight. However, the performance of the SMA spring varies according to the geometry and characteristics, such as the spring diameter, wire thickness, and number of spring turns (coils) [11], [12]. Therefore, it is necessary to configure an optimized SMA spring based on the desired displacement and installable space. In this study, the large-index-and-pitch (LIP) method was used to optimize the performance of an SMA spring [11], [12]. This method can determine the optimized number of coils such that the SMA can be repeatedly driven at a shear rate of 6% or less.

The maximum force generated according to the geometry and characteristics of the SMA spring can be expressed as follows:

$$F_{\max} = \frac{\pi d^3}{8D} G_A \gamma \tag{6}$$

where $F_{\max}$, d, D, G_A, and γ. denote the maximum force of the SMA spring, wire diameter, spring diameter, austenite shear modulus, and shear strain, respectively. The angle of each pitch of the SMA spring can be determined based on the extended length of the SMA spring. Therefore, the maximum displacement can be obtained if the maximum angle of each pitch is determined. The shear strain determined by the pitch angle is expressed as follows:

$$\gamma = \frac{1}{C} \frac{\cos^2\alpha_i(\sin\alpha_f - \sin\alpha_i)}{\cos^2\alpha_f(\cos^2\alpha_f + \sin^2\alpha_f/(1+\nu))} \tag{7}$$

where C, v, α_i, and α_f. are the spring index, Poisson's ratio, initial pitch angle, and final pitch angle, respectively. v is 0.33, because the SMA is assumed to be isometric. The maximum pitch angle was observed for martensite. In addition, depending on the number of coils and maximum pitch angle, the maximum displacement can be obtained as follows:

$$\delta_{dis} = \frac{\pi N D_i}{\cos\alpha_i}(\sin\alpha_f - \sin\alpha_i) \tag{8}$$

where N is the number of coils.

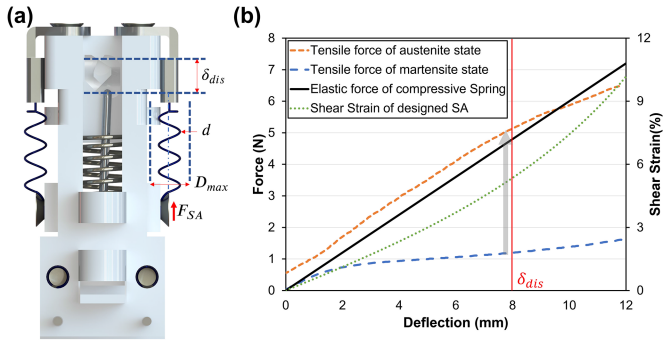

Fig. 3. (a) Configuration and geometry of the locking mechanism, (b) Relationship between deflection, tensile force, and shear strain for the (LIP) SMA coil actuator and used compressive spring observed by experiment. The SMA coil actuator has three coils with 7.2 spring index.

From the geometry of the mechanism in Fig. 3(a), the required displacement (δ_{dis}) and maximum coil diameter ($D_{\max}$) were obtained. In this study, as shown in Table I and Fig. 2(c), the parameters of mechanism used were 8 mm of the required displacement and 3 mm of maximum coil diameter. For operation, the SMA spring must be able to compress the compression spring using the required displacement. The used spring had a spring constant of 0.6 N/mm, and 4.8 N was required to move 8 mm.

The initial pitch angle was approximately 5° when the SMA spring was fully contracted. Using (7), the final pitch angle was calculated as 25° at 6% shear strain. In addition, by calculating the appropriate number of coils for a displacement of 8 mm using (8), 2.76 was obtained. Therefore, the number of coils of the SMA spring actuator was finally selected as three, and the performance of the actuator was observed through a linear experiment, as shown in Fig. 3(b).

In Fig. 3(b), the tensile forces and shear strain of the SMA spring actuator according to the deflection are shown. For the desired deflection of 8 mm, the SMA spring actuator could compress the spring with a higher force. In addition, the actuator could be optimized through a shear strain close to 6% at an 8 mm deflection. Furthermore, when the δ_{dis} is greater than 10 mm, an increase of N can make the overall system large. If N does not change, repeatability may decrease as 6% strain condition is not satisfied according to the LIP method [12], and the RLS malfunction because the $\boldsymbol{F}_{\max}$ is less than the force required to compress the spring.

C. Evaluating Performance of Retractable Locking System

As illustrated in Fig. 4, experiments were conducted to examine the operation of the presented RLS on the ratchet line and to prove the energy-saving effect of locking the RLS. As shown in Fig. 4(a), the ratchet line of the RLS was fixed on the rail of the linear guide, and the head part of the RLS was connected with a tendon to a load cell mounted on a linear robot that recorded its displacement by moving linearly using a step motor and an encoder. The other end of the head was connected to a load of 1 kg, and the force generated by pulling the load at a speed of 1 mm/s as the RLS moved over the ratchet line by the linear motion of the linear robot was measured in the load

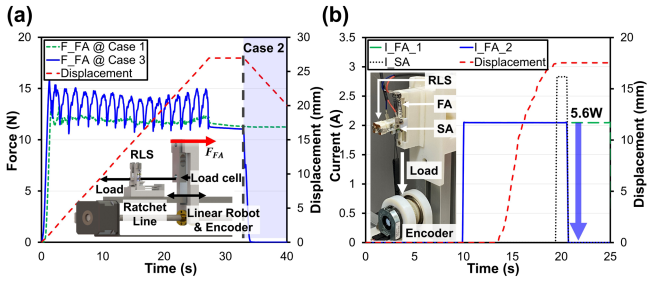

Fig. 4. Experimental setups and data to evaluate the performance of RLS (a) Force $\boldsymbol{F_{FA}}$ applied by pulling RLS and displacement data according to operational cases of RLS, (b) Setup to measure the energy saving of RLS and the current consumed to operate the FA pulling the RLS and its displacement.

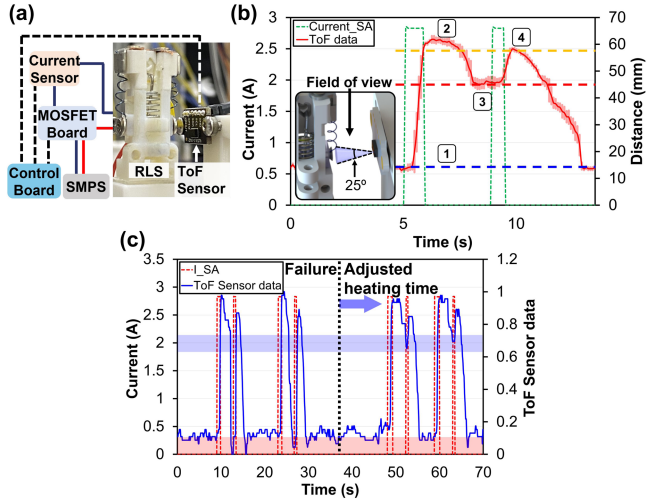

Fig. 5. (a) Configuration of the experimental equipment, (b) FoV of ToF sensor installed to determine state of RLS, current applied to SA and ToF sensor data, (c) Failure after repeatability experiment is resolved by adjusting the heating time.

cell as $\boldsymbol{F_{FA}}$ in (4). In Case 1, expressed as a green dashed line, the load acted as T_t in itself because the RLS was unlocked. In Case 3, expressed as a blue solid line, the load moved in a locked state, therefore the friction force between the pawl and ratchet line was added to the load and acted as a ripple in the graph. Moreover, by returning the linear robot to the original position, it was confirmed that $\boldsymbol{F_{FA}}$ becomes 0, while RLS remained locked state and becomes the Case 2 condition.

As shown in Fig. 4(b), an experiment was conducted to pull the RLS with a 1 kg load under two heating conditions of the FA to evaluate the energy-saving effect of the proposed RLS. The first condition was to continuously input a current of 2A to the FA for 15 s. Condition 2 was to input a current of 2A to the FA, when the RLS reached its maximum displacement, the SA was operated to change the RLS to a locked state and stop the FA from operating. By comparing $I_{\boldsymbol{FA}1}$ and $I_{\boldsymbol{FA}2}$ consumed by the FA in the two conditions, it was found that 5.6 W of power could be saved by locking the RLS. It was not necessary to continuously operate the FA to maintain a contracted state; therefore, not only energy saving was achieved but FA's failure by overheating could also be avoided.

In addition, the experimental equipment shown in Fig 5(a) was fabricated to evaluate the repeatability of RLS. Power was supplied to the SA in series and controlled by the MOSFET (IRF540N). The consumed current of SA was measured by a current sensor (INA219) and transmitted to a PC by a control board (Arduino Mega 2560). As shown in Fig. 5(b), one cycle of RLS operation is composed of two SA operations with 2.8 A current input, and the amount of electric energy consumed in one cycle was 12.47 J, which took a total of 6.4 s, consisting of 2.2 s for unlocking and 4.2 s for locking (first actuation: 0.8 s, cooling period: 1.4 s, second actuation: 0.5 s and cooling period: 3.5 s). The operating cycles was determined experimentally and can be shortened if cooling solutions such as fan are added to the system to produce a constant flow rate, and performance improvements based on cooling methods can be considered in future studies. Moreover, a time of flight (ToF) sensor was used to determine the failure of the repeatability experiments. The side of the RLS was measured as a distance data by the sensor, measuring change in the plane entering the field of view (FoV). Furthermore, ToF sensor data were defined by mapping the minimum and maximum values of the mean value of the distance data measured by five repetitions from 0 to 1 to determine the position of the pawl. As illustrated in Figs. 2(d) and 5(b), it can be confirmed that the ToF sensor data for each position of the hook was determined, and it can be evaluated whether the hook was well located at positions (1) and (3), which were the bistable positions in the repeated operation of the RLS switch.

Two sets of repetition experiments were performed 500 times each, and a failure occurred in the 877th time, in which the hook did not move to position (3). As shown in Fig. 5(c), during the operation after failure, hook was impossible to move to position (3) (red region), and by increasing the first heating time of the SA by 200 ms, the hook again reached position (3) (blue region) well. Since no mechanical damage was found in the system, and the failure was resolved through the adjustment of the heating time of the SMA, this operation failure is believed to be due to performance degradation from repetition of SA [19]. In future study, it is possible to monitor and feedback the current state of RLS by embedding a sensor in the hardware to control the heating time and solve the failure.

In addition, the ratchet line of RLS was in the form of teeth, and the lockable step was determined based on the spacing of the teeth. In Fig. 6, the distance that the pawl can move along the track is indicated by l_{track}. The actuation displacement of the actuator determines the usable track length. Therefore, l_{track} can be considered to be equal to the actuation displacement. The distance between the pitches of the teeth was l_{pitch}.

Here, the resolution indicates how detailed the locking section can be, and the smaller the number, the more locking sections can be implemented. The maximum resolution that the mechanism can achieve is obtained only when δ_{req} is equal to l_{track}. However, the displacement (δ_{req}) required to make the motion may be different from the maximum actuating range of the mechanism. δ_{req} must be less than l_{track} to achieve the desired behavior. When δ_{req} is less than l_{track}, the RLS resolution is

$$Resolution = \frac{l_{pitch}}{\delta_{req}} \tag{9}$$

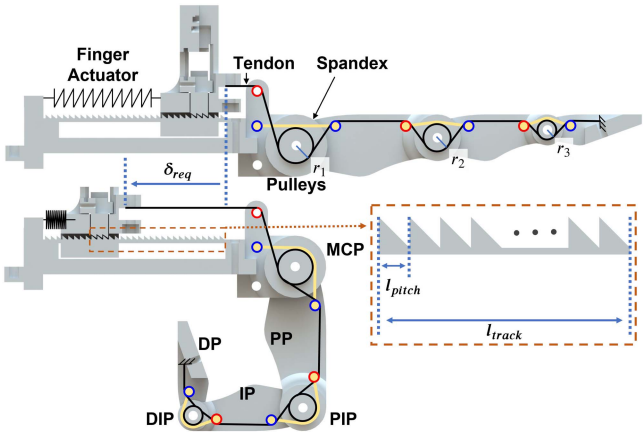

Fig. 6. Tendon routing diagram for full RoM of the finger and name of each joint part. Black line depicts the tendon path, yellow line depicts spandex to extend each joint and black circle depicts the pulleys to guide tendon. The finger includes three primary pulleys (Black circle) and three secondary pulleys (Red circle) for tendon drive. Each joint has additional pulleys (Blue circle) to wind spandex.

III. Finger With Retractable Locking System

A. Mechanism Design of Finger

An underactuated finger with a tendon structure was fabricated to evaluate the performance of the proposed locking system. Mankowski et al. broadly classified the finger structure of a robotic hand into eight categories [20], among these, an underactuated finger with a tendon structure has been used with various soft actuators, including motors, and is driven entirely by the tendon built into the fingers, making the structure simple and the fingers lightweight. This advantage allows the spring-type SMA, which has less force and moves linearly, to easily drive the finger. In designing the configurations of finger, the size of the standard finger for males aged 25–29 in the 6th year survey conducted by the Korean government was referenced [21].

Cabas et al. presented an optimization of the pulley position inside the link in the tendon-driven finger, and the tendon routing in this study referred to it [22]. A schematic of the tendon routing to be used in the proposed finger mechanism is shown in Fig. 6. This finger, like the human finger, consists of three primary joints of the metacarpophalangeal (MCP), proximal interphalangeal (PIP) and distal interphalangeal (DIP) joints, and three links of proximal phalange (PP), intermediate phalange (IP) and distal phalange (DP) connecting them. Furthermore, this finger has three primary pulleys as well as three secondary pulleys, and four additional pulleys (each joint has one primary pulley, one secondary pulley, and additional pulleys for the winding spandex to extend the joints). When analyzing this underactuated structure comprising a tendon and pulley, the force applied by the tendon is applied to the pulley to generate a moment in the joint, allowing it to rotate.

Lee et al. suggested that the radius of the joint is determined the actuator displacement [23]. The actuator displacement is limited by the size of the finger, limiting the maximum displacement. The maximum operational displacement of the actuator, considering the RLS and finger size, was 17 mm or less. According to a cadaveric study by Kapndji [24], which suggested that the range of motion (RoM) of human finger joints, assuming that each joint is rotated 90° by pulling the tendon and tendon is in constant contact with pulleys, the displacement of the tendon can be expressed as follows (r_1, r_2, and r_3 refer to the radius of a joint corresponding to three finger joints each as shown in Fig. 6):

$$\delta_{req} = \theta_{\max}\left(r_1 + r_2 + r_3\right) \tag{10}$$

Summarizing the equation under the above conditions and actuator contraction ratio, the sum of the radii must be less than 11 mm. Through this, the values of the radius are set as $r_1 = 4.5$ mm, $r_2 = 3.5$ mm, and $r_3 = 2.5$ mm. As the pulley radius decreases, the center distance between the rotation center of the joint and pulley increases; thus, the diameter of the commercial product is determined as a 2-mm shaft that can sufficiently withstand the force. In addition, the second pulley was set to a position where the tendon did not deviate from the joint when driving, thereby maintaining a constant magnitude of contraction displacement of the actuator.

The fineness of the finger angle was obtained based on the configuration of the designed finger and resolution calculated in Section II-C. According to (9) and (10), the angular step (θ_{step}) of the finger, to which locking can be applied, can be obtained as the product of the resolution and $\theta_{\max}$.

$$\theta_{step} = \frac{l_{pitch}}{\delta_{req}} \cdot \theta_{\max} = \frac{l_{pitch}}{r_1 + r_2 + r_3} \tag{11}$$

In this study, θ_{step} was 0.136 rad (7.81°). Therefore, assuming that the joints of the fingers rotate at the same angle to reach $\theta_{\max}$, 11 steps of locking can be applied at 7.81° intervals. According to (11), it is possible to change the fineness of the fingers by reducing the angle step by adjusting l_{pitch}, but there is a limitation owing to the mechanical characteristics of the ratchet line.

B. Structure for Antagonistic Motion

Human muscles act antagonistically, which means that when the muscles attached to both sides of the joint interact, one muscle bends the joint and the other stretches it, causing the joint to move bidirectionally. Usually, when a human lifts and holds an object, the joint stiffness is increased by applying force to the agonist and antagonist muscles [25]. Similar to a locking mechanism, the human body receives assistance from other organs when holding an object. For example, the human body assists the movement of the spine through intra-abdominal pressure during loading and unloading tasks [26]. Therefore, many biomimetic robots have been designed with antagonistic structures to exhibit motion similar to that of human muscles. However, the abovementioned fingers were flexed by the contractive force of the actuator, whereas active movement was difficult when stretched because they were actuated by the elastic force of the spring or elastic tendons when returning to their original position.

As shown in Fig. 7(a), in this study, a finger that can be actively driven in both directions by applying an antagonistic mechanism

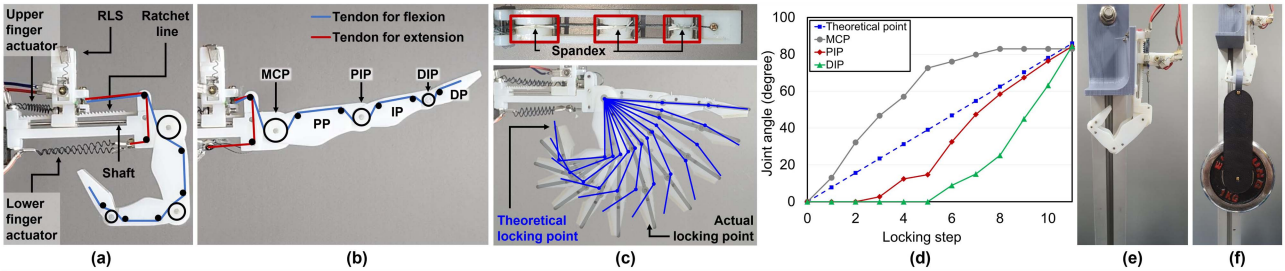

Fig. 7. Designed underactuated finger for SMA spring actuator. (a) Developed fingers comprising the RLS and underactuated structure and finger flexion, (b) Extension of finger, (c) Spandex fiber wound around the joint and speed difference of each joint flexion by the tension of the spandex (blue line: Theoretical finger flexion process according to locking step, black line: Actual finger flexion), (d) The theoretical finger joint angle bent along the displacement of the locking step of the RLS and the bending speed difference of each joint due to the tension of the spandex, (e) Lifting test of finger with the RLS, and (f) Under 3-kg load.

TABLE II
COMPARISON OF LOCKING SYSTEM FOR SOFT ROBOTIC APPLICATION

Index	This work	Saharan et al. [14]	Park et al. [15]	Hu et al. [16]
Num of stable position	2	1	1	1
Locking force	30 N (w/ finger)	4 N	80 N	27.5 N
Response speed (Unlocking/ locking)	2.2 s / 4.2 s	15 s ~	5 s / 1.5 s	-
Energy consumption	12.47 J	112.5 J	63 J	-

is fabricated. The proposed finger also comprises two pairs of actuators: upper finger actuators (UFA), which bend the finger, and lower finger actuators (LFA), which stretch it. An UFA, with one end connected to the finger body and the other end connected to the RLS, pulls it during contraction, and the tendon from the RLS is fixed to the DP, which causes the fingers to bend when the RLS moves. Therefore, when the UFA is operated, the joints are bent along the displacement generated by the RLS moving according to the locking step. In contrast, the LFA is not connected to the DP, but is directly connected to the RLS through the tendon. This design addresses the frictional force problem that occurs when the actuator is connected to the DP, and directly moves the RLS when operating the LFA.

Therefore, when the UFA contracts when heated, the RLS moves backward, relaxing the bottom actuator using the connected tendon and bending the fingers (Fig. 7(a)). By contrast, when the LFA is heated and contracts, the UFA is stretched under the same principle, and the RLS returns to place (Fig. 7(b)). In addition, the pulling tendon loosens, and the fingers are stretched by the spandex fiber over each joint. Through this structure, when the RLS is locked state, the finger can maintain bending and lift heavy objects. When unlocked, the fingers can be extended by operating an LFA.

C. Performance of Finger With Retractable Locking System

The finger under the application of the RLS was 158.9 mm in total length, 88.9 mm in finger length, 44 mm in height, 14 mm in width, and 30 g in weight. All parts of the finger were fabricated using a 3D printer (Objet 24, STRATASYS Co., Vero White). Each joint was connected by a 2-mm pin shaft, and a spandex was used for the extension (Fig. 7(c)). Moreover, the tension of each joint depends on the number of spandex windings, and the tension in the DIP is the strongest and the MCP is the smallest ($T_{DIP} > T_{PIP} > T_{MCP}$). In addition, the tension difference between the presented finger joints caused the actual finger joints to reach the maximum angle in order of MCP, PIP, and DIP (Fig. 7(c)), unlike the theoretical model in which all joints rotate together according to the θ_{step} obtained by (11), thus to implement an adaptive grip suitable for wrapping an object.

The designed fingers were driven by spring-type SMA (artificial muscle, Flexinol Co, spring diameter: 3.45 mm and wire diameter: 0.51 mm, number of coils: 10) at both UFA and LFA. The operation time of the finger driven by FA with 2.8 A current applied is 2 s for flexion and 2.6 s for extension, and 3.2 s for flexion while the RLS is locked. A lifting test of the fingers using the system was conducted to determine the effectiveness of the developed RLS. As long as the locked fingers were not released, the actuator maintained a contracted state, and the fingers remained bent. For the lifting test, an experiment was conducted using the fingers, excluding the bottom actuator. In the experiment, 1-, 2-, and 3-kg plates were placed on the fixed fingers sequentially and held for 5 min. Fig. 7(d) shows the initial state, in which the actuator is contracted and locked. Fig. 7(e) shows the placement of the plates on the finger. The experimental results confirmed that the finger could lift up to 3 kg of weight. However, as the load increased, the fingers fixed by the RLS were bent, and the PP part broke when more than 4 kg of the load was hung.

IV. CONCLUSION

In this study, the designed retractable locking system overcame the limited force of the SMA spring actuator. Despite the high strain and flexibility of the SMA spring actuator, its usability in robotics has been limited owing to less force than conventional actuators such as motors. In addition, because of the characteristics of the SMA actuator, which cannot exert force without the application of heat, it has a disadvantage of not being able to hold or maintain a contraction without continuous energy consumption. The ratchet-applied RLS was applied to the fingers to compensate for these shortcomings, which allowed

the fingers to remain bent by maintaining the actuator retraction without additional power consumption. In addition, because of the application of the retractable structure, the locking system exhibited two independent states (locked and unlocked), and the actuator only needed to be driven during the lock–unlock operation. Compared to previous soft robotic applications of locking systems, as shown in Table II, the developed RLS has bistability, meaning, it can switch between two states with one actuation, unlike other similar performance system. Therefore, since the proposed RLS implements locking/unlocking states using a structure in which two stable positions are maintain without power consumption, RLS consumes significantly less energy and has faster response time than other studies. However, because of the complex structure of RLS compared to other studies, it is likely to be weak against high repetitions. Therefore, the developed RLS proved the robustness of the system through more than 800 reps of consecutive repeated experiments, but the failure due to performance degradation of SMA occurred in the 877th operation, which was resolved through heating time adjustment. In the future, further reliability could be improved by embedding sensor in RLS that can monitor the switching of the two stable states.

Furthermore, unlike previous studies, there is a difference in that when the actuator contracts in the locked state, the fingers are bent, during the RLS remains in a locked state without unlocking [14], [15]. Finally, a lightweight robot finger with RLS driven by a spring-type SMA capable of lifting 3 kg of objects was manufactured. The proposed system operates on linear motion and has a simple way of connecting loads and actuators to both ends of the system; therefore, it can be applied to other linear actuators as well as heat-based actuators, such as SMA or DTCA, which will be further investigated. The proposed RLS can be easily applied, particularly for systems that operate soft robot hands with a limited number of actuators or that transmit force on a tendon-driven mechanism [27].

In the future, the effectiveness of the proposed RLS will be explored by applying a locking system to a life-scale linear pneumatic actuator-based robot arm. In addition, we will attach the RLS to the actuator surface of the fabric wearable robot and attempt to implement the function of the sensor and energy management by allowing the ratchet line to function as an encoder.

REFERENCES

[1] S. Mirvakili and I. Hunter, "Artificial muscles: Mechanisms, applications, and challenges," *Adv. Mater.*, vol. 30, no. 6, 2017, Art. no. 1704407.

[2] K. Kim et al., "Double helix twisted and coiled soft actuator from spandex and nylon," *Adv. Eng. Mater.*, vol. 20, no. 11, 2018, Art. no. 1800536.

[3] Y. Chung, J. Lee, J. Jang, H. Choi, and H. Rodrigue, "Jumping tensegrity robot based on torsionally prestrained SMA springs," *ACS Appl. Mater. Interfaces*, vol. 11, no. 43, pp. 40793–40799, 2019.

[4] A. Sofla, S. Meguid, K. Tan, and W. Yeo, "Shape morphing of aircraft wing: Status and challenges," *Mater. Des.*, vol. 31, no. 3, pp. 1284–1292, 2010.

[5] J. Shintake, S. Rosset, B. E. Schubert, D. Floreano, and H. R. Shea, "A foldable antagonistic actuator," *IEEE/ASME Trans. Mechatron.*, vol. 20, no. 5, pp. 1997–2008, Oct. 2015.

[6] J. D. W. Madden et al., "Artificial muscle technology: Physical principles and naval prospects," *IEEE J. Ocean. Eng.*, vol. 29, no. 3, pp. 706–728, Jul. 2004.

[7] B. Yoon, J. Park, and K. Yoon, "Experimental study on control fins of a small flying vehicle using piezo-composite actuators," *Adv. Composite Mater.*, vol. 26, no. 1, pp. 35–43, 2016.

[8] H. Jung et al., "Design and fabrication of twisted monolithic dielectric elastomer actuator," *Int. J. Control, Automat. Syst.*, vol. 15, no. 1, pp. 25–35, 2017.

[9] D. Hartl, J. Mooney, D. Lagoudas, F. Calkins, and J. Mabe, "Use of a Ni60Ti shape memory alloy for active jet engine chevron application: II. Experimentally validated numerical analysis," *Smart Mater. Structures*, vol. 19, no. 1, 2009, Art. no. 015021.

[10] K. Cho et al., "Sliding filament joint mechanism: Biomimetic artificial joint mechanism for artificial skeletal muscles," *J. Mechanisms Robot.*, vol. 11, no. 2, 2019, Art. no. 021004.

[11] S. An, J. Ryu, M. Cho, and K. Cho, "Engineering design framework for a shape memory alloy coil spring actuator using a static two-state model," *Smart Mater. Structures*, vol. 21, no. 5, 2012, Art. no. 055009.

[12] J. S. Koh and K. J. Cho, "Omega-shaped inchworm-inspired crawling robot with large-index-and-pitch (LIP) SMA spring actuators," *IEEE/ASME Trans. Mechatron.*, vol. 18, no. 2, pp. 419–429, Apr. 2013.

[13] M. Plooij, G. Mathijssen, P. Cherelle, D. Lefeber, and B. Vanderborght, "Lock your robot: A review of locking devices in robotics," *IEEE Robot. Automat. Mag.*, vol. 22, no. 1, pp. 106–117, Mar. 2015.

[14] L. Saharan and Y. Tadesse, "Robotic hand with locking mechanism using TCP muscles for applications in prosthetic hand and humanoids," *Proc. SPIE*, vol. 9797, 2016, pp. 178–186.

[15] S. Park, J. Jeong, M. Won, and C. Park, "Locking–unlocking mechanism actuated by SMA springs to improve the energy efficiency of fabric-type soft actuators," *Smart Mater. Structures*, vol. 28, no. 12, 2019, Art. no. 125005.

[16] Q. Hu, H. Huang, E. Dong, and D. Sun, "A bioinspired composite finger with self-locking joints," *IEEE Robot. Automat. Lett.*, vol. 6, no. 2, pp. 1391–1398, Apr. 2021.

[17] Y. Cao, M. Derakhshani, Y. Fang, G. Huang, and C. Cao, "Bistable structures for advanced functional systems," *Adv. Funct. Mater.*, vol. 31, no. 45, 2021, Art. no. 2106231.

[18] S. S. Groothuis, R. Carloni, and S. Stramigioli, "Single motor-variable stiffness actuator using bistable switching mechanisms for independent motion and stiffness control," in *Proc. IEEE Int. Conf. Adv. Intell. Mechatron.*, 2016, pp. 234–239.

[19] H. Zhou, S. Cao, and N. Ma, "Design and performance analysis of a novel class of SMA-driven rotational mechanisms/joints," *Robotica*, vol. 40, no. 11, pp. 3976–3994, 2022.

[20] T. Mańkowski, J. Tomczyński, K. Walas, and D. Belter, "PUT-hand—Hybrid industrial and biomimetic gripper for elastic object manipulation," *Electronics*, vol. 9, no. 7, 2020, Art. no. 1147.

[21] "Size Korea (Korean human body dimension survey)," Sizekorea.kr, 2021. Accessed: 10, Dec. 2020. [Online]. Available: https://sizekorea.kr/measurement-data/hand

[22] R. Cabas, L. M. Cabas, and C. Balaguer, "Optimized design of the underactuated robotic hand," in *Proc. IEEE Int. Conf. Robot. Automat.*, 2006, pp. 982–987.

[23] G. Lee and Y. Choi, "Bio-inspired tendon-driven finger design with isomorphic ligamentous joint," *IEEE Access*, vol. 8, pp. 18240–18251, 2020.

[24] A. I. Kapandji, *The Physiology of the Joints*, vol. 1. London, U.K.: Churchill Livingstone, 2007.

[25] C. De Luca and B. Mambrito, "Voluntary control of motor units in human antagonist muscles: Coactivation and reciprocal activation," *J. Neurophysiol.*, vol. 58, no. 3, pp. 525–542, 1987.

[26] N. Arjmand and A. Shirazi-Adl, "Role of intra-abdominal pressure in the unloading and stabilization of the human spine during static lifting tasks," *Eur. Spine J.*, vol. 15, no. 8, pp. 1265–1275, 2005.

[27] S. Yang et al., "Design and control of lightweight bionic arm driven by soft twisted and coiled artificial muscles," *Soft Robot.*, to be published doi: https://doi.org/10.1089/soro.2021.0058.